Conjugated Dual Hydrogen-Bond Mediating Proton-Transfer Reaction in 3-Hydroxyisoquinoline

Ching-Yen Wei, Wei-Shan Yu, and Pi-Tai Chou*

Department of Chemistry, The National Chung-Cheng University, Chia Yi, Taiwan, ROC

Fa-Tsai Hung

The National Hu-Wei Institute of Technology, Yunlin, Taiwan, ROC

Chen-Pin Chang and Te-Cheng Lin

Department of Chemistry, Fu Jen Catholic University, Shin Chuang, Taiwan, ROC

Received: September 30, 1997; In Final Form: November 11, 1997

Proton-transfer tautomerism mediated by the conjugated dual hydrogen-bonding (CDHB) effect in the ground state as well as in the excited state has been studied in 3-hydroxyisoquinoline (3HIQ). In cyclohexane, upon increasing concentration or adding guest molecules possessing the bifunctional hydrogen-bonding property, spectral and dynamic analyses indicate the existence of equilibria between various proton-transfer tautomers, including enol monomers, enol dimers (or 1:1 enol/guest complex), and keto/enol complexes (or 1:1 keto/guest complexes). The equilibrium constants among each species have been determined, which can be qualitatively rationalized through an ab inito molecular orbital calculation. The results conclude that the CDHB formation and its strength play a key role to fine-tune the ground-state equilibria toward the keto form. Upon excitation the enol CDHB complexes undergo a rapid proton-transfer reaction ($k_{pt} \gg 5 \times 10^9$ s^{-1}), resulting in a unique keto emission. Surprisingly, however, drastically different excited-state relaxation dynamics between the keto dimer and keto/enol complex were observed. The result was tentatively rationalized by a deactivation mechanism induced by vibrations of low-frequency hydrogen-bonding modes associated with the CDHB strength.

Introduction

At the molecular level, one possible mechanism for the mutation has been proposed to be, in part, due to a "misprint" induced by the proton-transfer tautomerism of a specific DNA base during replication, and then an error is recorded.[1−3] Based on this fundamental concept, studies on proton-transfer tautomerism mediated by the hydrogen-bonding effect have been one of the focal areas for the past three decades. Among numerous studies, the tautomerism between 2-hydroxypyridine (HP) and its keto tautomer 2-pyridone (PD) is a prototype. The keto−enol equilibrium mediated by the PD hydrogen-bonded dimer has been extensively investigated.[4−17] Recently, based on a higher-level ab initio approach, our studies have shown that equilibrium between PD and HP can be fine-tuned not only by self-association but also by association with the guest molecules through conjugated dual hydrogen-bonding (CDHB) formation.[18] (The term of CDHB is defined as a dual hydrogen-bonding formation in which both proton donating and accepting sites can be induced resonantly.) Unfortunately, the photophysical properties such as absorption, emission spectra, and relaxation dynamics between monomers and their corresponding dimers and/or complexes are similar. This in combination with the existence of an intrinsic equilibrium between PD and HP monomers in gas as well as solution phase makes the experimental determination of equilibria mediated by the CDHB effect difficult. To overcome such an obstacle, we have searched for potential compounds exhibiting similar CDHB behavior, while both thermodynamic and dynamic properties can be resolved spectroscopically. It turns out that 3-hydroxyisoquinoline (3HIQ; see Figure 1), having a subunit analogous to HP, is an ideal model to study the proton-transfer tautomerization mediated by the CDHB effect. In aqueous solution 3HIQ exists exclusively as a keto form, while the enol form is the predominant species in the diluted gas phase and hydrocarbon solvents. In cyclohexane, upon increasing concentration or adding guest molecules possessing bifunctional hydrogen-bonding properties, spectral and dynamic analyses indicate the existence of equilibria between various proton-transfer tautomers, including enol monomers, enol dimers (or 1:1 enol/guest complex), and enol/keto complexes (or 1:1 keto/guest complexes), which all exhibit quite different photophysical behaviors. Thus, thermodynamic properties among various hydrogen-bonding species can be determined experimentally.

The following sections are organized according to a sequence of steps where we first performed absorption titration experiments and derived a series of association equations to determine the equilibrium constants for various 3HIQ CDHB species in cyclohexane. The next step involved steady-state and time-resolved fluorescence measurements to examine the excited-state proton-transfer properties. The results were qualitatively rationalized by a subsequent theoretical approach. Finally, the enol−keto proton-transfer equilibria and the excited-state relaxation dynamics fine-tuned by the CDHB strength will be elaborated in the Discussion section.

* To whom correspondence should be addressed.

S1089-5647(97)03173-8 CCC: $15.00
Published on Web 01/16/1998

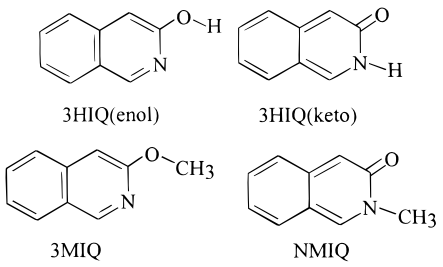

Figure 1. Structures of the proton-transfer isomers and derivatives of 3HIQ.

Experimental Section

Materials. 3HIQ (Aldrich) was purified by column chromatography **(**eluent 3:1 hexane/ethyl acetate). The purity was checked by the fluorescence excitation spectrum in cyclohexane under a sufficiently low concentration of $<10^{-6}$ M, where the enol form exists predominantly. 3-Methoxyisoquinoline (3MIQ) and *N*-methyl-3-isoquinolone (NMIQ; see Figure 1) were synthesized according to the previously reported method.[19] The final products were twice recrystallized from spectragrade ethanol and once from cyclohexane. Acetic acid (ACID, Merck Inc.) and 2-azacyclohexanone (ACH, Aldrich) were purified on the basis of the previously described method.[20] Triethylamine (TEA, Aldrich) was used without further purification because no interference of the impurity fluorescence was detected in the wavelength region of interest. Cyclohexane (Merck Inc.) was of spectragrade quality and was refluxed several hours over lithium aluminum hydride under a nitrogen atmosphere and was transferred, prior to use, through distillation to the sample cell.

Measurements. Steady-state absorption and emission spectra were recorded by a Cary 3E (Perkin-Elmer) spectrophotometer and a Hitachi (SF4500) fluorimeter, respectively. The excitation light source of the fluorimeter has been corrected by the Rodamine B spectrum. In addition, the wavelength-dependent characteristics of the monochromator and photomultiplier have been calibrated by recording the scattered light spectrum of the corrected excitation light from a diffused cell in the range 220−700 nm. Both absorption and emission data were transferred to the Origin 4.1 (Microcal Software, Inc.) software package for further analyses. Lifetime studies were performed by an Edinburgh FL 900 photon-counting system with a hydrogen-filled flash lamp/or a nitrogen lamp as the excitation source. The temporal resolution after deconvolution of the excitation pulse was 200 ps. The data were analyzed using a nonlinear least-squares fitting program with a deconvolution method reported previously.[21]

Theoretical Calculations. The methodology of the theoretical calculation was carried out on the basis of following sequences. The initially optimized structure used for the ab initio calculation was obtained by the semiempirical AM1 method using a Spartan package (Release 3.1.6, Wavefunction, Inc., Irvine, 1994) on a SiliconGraphics workstation. Ab initio molecular orbital calculations were performed by using Gaussian 94 Rev D.3 programs. Geometry optimizations for all structures were carried out with the 6-31G* basis set at the Hartree−Fock (HF) level. This basis set has proven to be suitable for the dimer (or complex) formation incorporating hydrogen-bonding formation.[22] It is certainly necessary to check whether the optimized geometrical structure for those dimeric and complex forms is at an energy minimum, transition state, or higher-order saddle point. Therefore, the Hessians, and hence vibrational frequencies, were calculated, and the result shows no imaginary vibrational frequencies for all 3HIQ CDHB complexes studied. The directly calculated zero-point vibrational energies (ZPE) were scaled by 0.9181[23] to account for the overestimation of vibrational frequencies at the HF level. We also attempted to extract energy factors solely associated with the hydrogen-bonding effect. Hence the association energy, ΔH_{ac}, was calculated as the change in the total molecular enthalpy of formation in the conversion of the optimized monomer individually into the optimized dimer. However, this procedure involves certain inconsistencies due to the basis-set superposition (BSSE) and has been corrected by a counterpoise correction procedure[24−26] in which the energy of the monomer was calculated by adding ghost atoms in space to the dimer and/or complex, corresponding to the equilibrium positions of the counterpart monomer, that is $\Delta H_{ac} = [H(\text{dimer or complex}) - 2H(\text{monomer}) - \Delta E_{cp}(\text{BSSE})]$, where ΔE_{cp}(BSSE) denotes the monomer energy corrected by the counterpoise correction procedure.

Hydrogen-Bonding Equilibria

3HIQ Self-Association. Figure 2 shows the concentration-dependent absorption spectra of 3HIQ in cyclohexane. When the concentration was prepared as low as 5.0×10^{-6} M in cyclohexane, similar to that observed by Evans et al.,[19] 3HIQ exhibits an S_0-S_1 absorption band with a structural vibronic progression maximum at ∼340 nm. However, upon increasing the concentration, a previously unrecognized spectral feature appears in the region of >350 nm, where a shoulder grows in the region of 350−380 nm accompanied by the observation of a weak absorption band maximum at ∼420 nm. In comparison, 3MIQ is generally treated as an enol model in which the enol−keto tautomerism is prohibited due to its lack of a hydroxyl proton. In addition, the lack of the hydroxyl proton also prevents the formation of any hydrogen-bonded dimer and/or complex. The S_0-S_1 absorption maximum of 3MIQ was measured to be at ∼330 nm in cyclohexane. The spectral feature is concentration-independent and is similar to that of 3HIQ when the concentration was prepared as low as 5×10^{-6} M. We thus conclude that at a sufficiently low concentration 3HIQ exists mainly as the enol monomer form. To characterize other species in the equilibria, a keto form-like tautomer *N*-methyl-3-isoquinolone (NMIQ, see Figure 1) has been synthesized, which exhibits an S_0-S_1 absorption maximum at ∼410 nm. Because of its spectral resemblance with respect to the NMIQ emission, we tentatively ascribe the observed 420-nm band in concentrated 3HIQ to the S_0-S_1 absorption of a keto-like tautomer. However, the concentration-dependent growth of the 420-nm band leads us to conclude this species to be an associated form. Theoretically, two possible keto-like forms based on the formation of a 1:1 hydrogen-bonded complex can be derived: namely, the keto dimer and keto/enol complex. Both can give rise to the 420 nm absorption band associated with the keto chromophore. At this stage, a definitive conclusion cannot be made simply based on the absorption spectroscopy. In the later section, however, both excited-state relaxation dynamics and theoretical approaches will draw the same conclusion that the keto/enol complex rather than the keto dimer exists predominantly in the equilibria.

In comparison to the absorption spectrum of NMIQ, in which the absorption in the region of 350 nm is tailing down to a minimum, the growth of the 350-nm absorption band in 3HIQ upon increasing the concentration is not likely to be mainly ascribed to the keto absorption. On the other hand, since the correlation between the concentration-dependent 350- and 420-

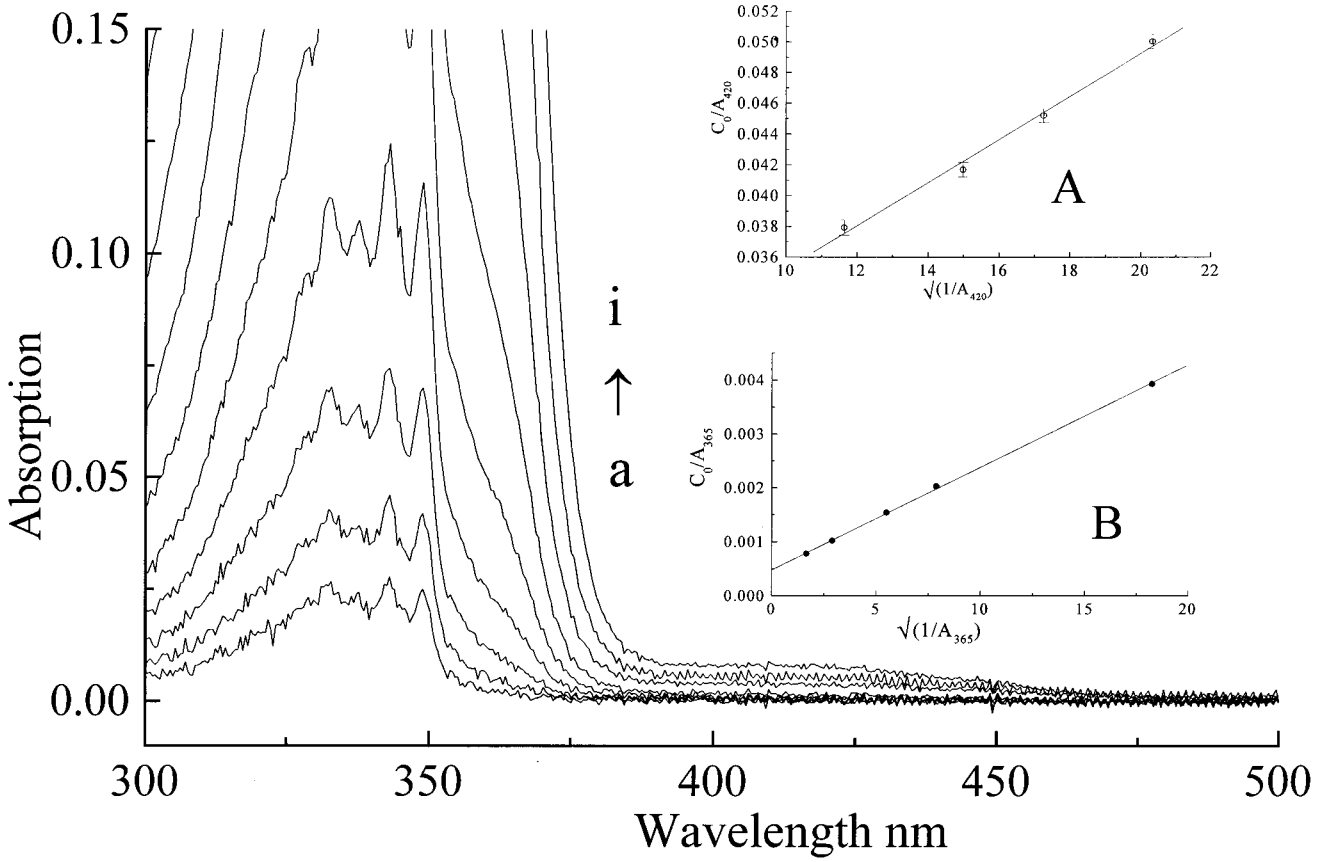

Figure 2. The concentration-dependent absorption spectra of 3HIQ in cyclohexane, in which 3HIQ was prepared at (a) 7.30×10^{-6}, (b) 1.18×10^{-5}, (c) 2.00×10^{-5}, (d) 3.26×10^{-5}, (e) 5.09×10^{-5}, (f) 7.86×10^{-5}, (g) 1.21×10^{-4}, (h) 1.85×10^{-4}, and (i) 2.8×10^{-4} M. Inset A: Plot of C_0/A_{420} values against the square root of $1/A_{420}$. Inset B: Plot of C_0/A_{365} versus the square root of $1/A_{365}$. The definitions of C_0, A_{420}, and A_{365} have been given in the text.

nm bands is not linear (vide infra), it is also unlikely that the 350-nm band can be mainly attributed to the hydrogen-bonded enol part of the keto/enol CDHB complex. Furthermore, in the case of 3MIQ, a similar concentration-dependent red-shifted absorption spectrum was not observed. Therefore, the 350-nm absorption band resulting from a non-hydrogen-bonding solvatochromism of the enol monomer can be excluded. We thus tentatively assign this species to the enol dimer form in which the S_0-S_1 absorption is red-shifted with respect to the enol monomer due to the CDHB formation. Further detailed discussion and confirmation of this assignment will be given in later sections.

On the basis of above results, at a relatively high concentration of 3HIQ, two competitive equilibria among the enol monomer, the enol dimer, and the keto/enol complex were established and are depicted in Scheme 1,

Scheme 1

$$2\ \text{enol} \overset{K_a}{\rightleftharpoons} (\text{enol})_2 \overset{K_b}{\rightleftharpoons} (\text{keto/enol})$$

where K_a is the association constant for the enol dimer, K_b is the equilibrium constant between the enol dimer and the keto/enol complex. Since at sufficiently long wavelengths, for example, 420 nm, the absorption is attributed exclusively to the keto/enol complex, one can incorporate the Beers−Lambert law for the keto/enol complex and write

$$A_{420} = \epsilon_{420}[\text{keto}]l \qquad (3)$$

where A_{420} is the absorbance at 420 nm, ϵ_{420} is the molar extinction coefficient of the keto form at 420 nm, and l is the path length of the cell. Combining Scheme 1 and eq 1 leads to eq 2 depicted as

$$\frac{C_0}{A_{420}} = \sqrt{\frac{1}{\epsilon_{420} l K_b K_a}}\sqrt{\frac{1}{A_{420}}} + \frac{2}{\epsilon_{420} l}\left(\frac{1}{K_b} + 1\right) \qquad (2)$$

where C_0 is the actual concentration of 3HIQ in the solution, and l was fixed to 1.0 cm throughout the study. Inset A of Figure 2 illustrates the application of eq 2 to data obtained at 420 nm in cyclohexane. Plotting C_0/A_{420} against the square root of $1/A_{420}$ gives sufficiently linear behavior to support the assumption of a 1:1 complex for both the enol dimer and the enol/keto complex. The best fit using eq 2 gives the slope and intercept to be 1.39×10^{-3} and 3.3×10^{-2} M, respectively. To extract K_a and K_b, additional information for the ϵ_{420} value of the keto form is required. Due to the lack of available data, we have to make a rational estimation. In one experiment, the ϵ_{420} value of the synthesized keto-like compound, NMIQ, has been determined to be 2970 M^{-1} cm^{-1} at 420 nm in cyclohexane. On the other hand, for 3HIQ in water where the keto form is a predominant species, ϵ_{420} has been determined to be 2850 M^{-1} cm^{-1}. We simply take the average of these two measured ϵ_{420}, giving a mean value of 2910 M^{-1} cm^{-1}, for the keto/enol complex in cyclohexane. Accordingly, K_a and K_b were calculated to be 8.5×10^3 and 0.021, respectively. Since the result indicates that only a trace of the keto form exists in the equilibria, we can neglect the keto/enol complex formation and attribute the absorption in the region of 365 nm to the S_0-S_1 transition of the enol dimer. Therefore, the relationship between the initially prepared 3HIQ concentration, C_0, and the measured

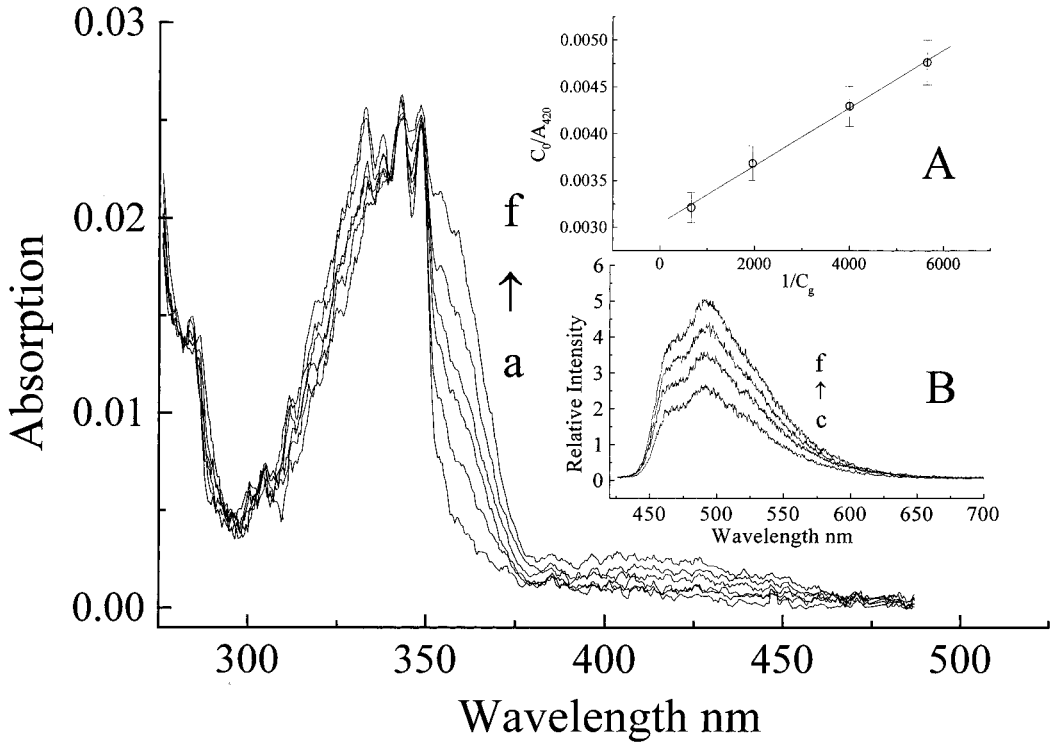

Figure 3. Concentration-dependent absorption spectra of 3HIQ (5.0×10^{-6} M) in cyclohexane by adding various ACID concentrations (C_g) of (a) 0, (b) 4.33×10^{-5}, (c) 1.10×10^{-4}, (d) 1.77×10^{-4}, (e) 5.10×10^{-4}, and (f) 1.51×10^{-3} M. Inset A: Plot of C_0/A_{420} against $1/C_g$ and the best fit straight line. Inset B: Fluorescence spectra as a function of C_g which was prepared to be the same as c → f. The excitation wavelength was 365 nm.

absorbance at 365 nm, A_{365}, can be simplified to eq 3.

$$\frac{C_0}{A_{365}} = \sqrt{\frac{1}{\epsilon_{365} l K_a}}\sqrt{\frac{1}{A_{365}}} + \frac{2}{\epsilon_{365} l} \tag{3}$$

The plot of C_0/A_{365} versus the square root of $1/A_{365}$ gives a straight line (see inset B of Figure 2). ϵ_{365} of the enol dimer, extracted from the intercept, was calculated to be 3250 cm^{-1} M^{-1}. Using the slope, K_a was calculated to be 7.82×10^3, which, within experimental error, is consistent with that obtained from eq 2. This result supports the validity of the assumption that the enol dimer is a dominant species in the self-association. The K_a value of 8.5×10^3 corresponds to a $\Delta G°$ value of −5.36 kcal/mol at room temperature. This value is much stronger than would be anticipated simply from the number and type of hydrogen bonds involved. For example, the pyrrole−pyridine complex was reported to have $\Delta G°$ values of −1.9 kcal/mol.[27] Fritzche reported a $\Delta G°$ value of 0.81 kcal/mol for the indole−pyridine complex in CCl_4.[28] Therefore, the unusually large association constant for the 3HIQ enol dimer suggests a cooperative change in the electronic configuration of the enol (or keto) form mediated by the CDHB formation, resulting in a significant red shift of the S_0-S_1 transition. Further support for this viewpoint will be given in the theoretical calculation section. The value of $\Delta G°$ for the $(enol)_2$ → (keto/enol) isomerization, according to a K_b value of 0.021, was calculated to be 2.29 kcal/mol. However, it should be noted that $\Delta G°$ associated with the $(enol)_2$ → (keto/enol) tautomerism involves the conversion of the monomeric enol to the keto species intrinsically. Therefore, further information regarding the relative stability between the enol and keto forms has to be known in order to extract the energy associated with the CDHB formation (vide infra). An attempt to measure the temperature-dependent K_a and K_b as a function of temperature in order to extract the association enthalpy, ΔH_{ac}, of the reaction unfortunately failed due to the sparse solubility of 3HIQ at low temperature. Nevertheless, a detailed discussion of ΔH_{ac} based on a theoretical approach and its correlation with respect to the hydrogen-bonding strength will be elaborated in the section on theoretical calculations.

3HIQ/Guest CDHB Complexes. The CDHB effect on the proton-transfer tautomerization can be illustrated not only by the 3HIQ self-association form but also in various 3HIQ/guest CDHB complexes. In this study, two guest molecules, acetic acid (ACID) and 2-azacyclohexanone (ACH), were selected, possessing the carboxylic acid and amide bifunctional hydrogen-bonding sites, respectively. Figure 3 shows the absorption spectra of 3HIQ upon adding the acetic acid in cyclohexane. In this experiment, the initial concentration of 3HIQ, C_0, was prepared as low as 5.0×10^{-6} M to avoid self-dimerization. The equilibria between various species due to the CDHB formation are clearly indicated by the growth of ∼350- and 420-nm bands throughout the titration, corresponding to the equilibria among enol monomer, enol/ACID, and keto/ACID CDHB complexes. A generalized association mechanism can be depicted as

$$\text{enol} + \text{guest} \overset{K_a}{\rightleftharpoons} \text{enol/guest} \overset{K_b}{\rightleftharpoons} \text{keto/guest}$$

Similarly, the absorbance peak at 420 nm can be exclusively attributed to the S_0-S_1 absorption of the keto/ACID CDHB complex. Therefore, the relationship between the initially prepared acid concentration, C_g, and the measured absorbance at 420 nm, A_{420}, can be expressed in eq 4.

$$\frac{C_0}{A_{420}} = \frac{1}{\epsilon_{420} l K_a K_b}\frac{1}{C_g} + \frac{K_b + 1}{\epsilon_{420} l K_b} \tag{4}$$

TABLE 1: Photophysical Properties of 3HIQ Hydrogen-Bonding Species in Cyclohexane

	absorption $S_0 \rightarrow S_1$(nm)	k_a and k_b (ΔG kcal/mol)	fluorescence (nm)	τ_{obs} (ns)	Φ_f[a]
self-association	340 (enol)		370 (enol)	6.62 (enol)	0.27 (enol)
	350 (enol/enol)	k_a: 8.5×10^3 (−5.36)	490 (keto/enol),	6.34 (keto/enol)	0.142 (keto/enol)
	425 (keto/ enol)	k_b: 0.021(2.29)	(keto/keto)	0.58 (keto/ keto)	0.013 (keto/ keto)
ACID	350 (enol/ACID)	k_a: 1.2×10^4 (−5.56)	490 (keto/ACID)	7.05 (keto/ACID)	0.143 (keto/ACID)
	420 (keto/ACID)	k_b: 0.15 (1.12)			
ACH	345 (enol)	k_a: 3.2×10^3 (−4.78)	500 (keto/LIM),	8.3 (keto/LAM),	0.106[b] (keto/LAM),
	430 (keto/LAM)	k_b: 0.10 (1.36)	(keto/LAM)	(keto/LIM)	(keto/LIM)

[a] The quantum yield of the keto form was determined by the assumption that the excited-proton-transfer reaction is an adiabatic and dominant process. [b] The spectral properties for keto*/LAM and keto*/LIM species are indistinguishable (see the text for a detailed description).

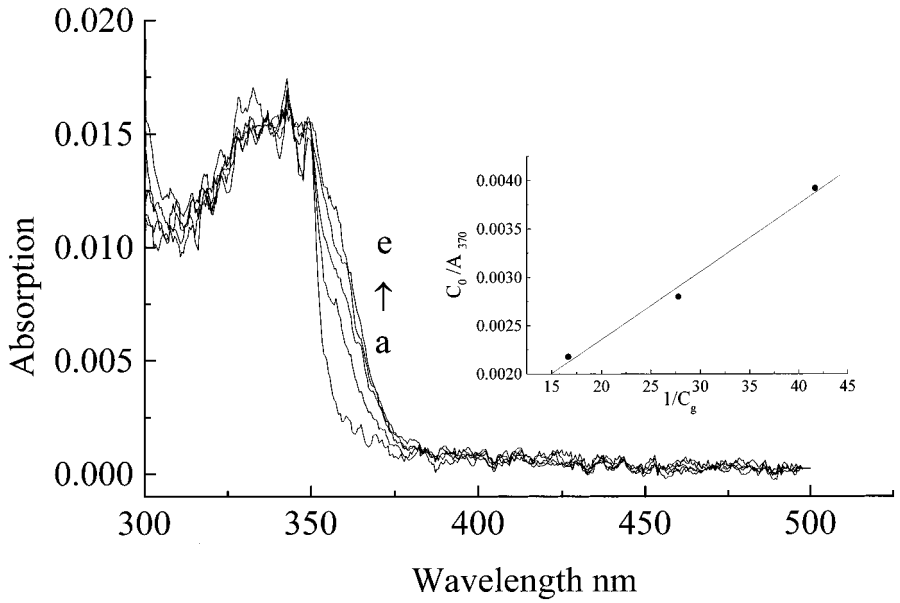

Figure 4. Concentration-dependent absorption spectra of 3HIQ (5.0×10^{-6} M) in cyclohexane by adding various triethylamine (TEA) concentrations (C_g) of (a) 0, (b) 7.2×10^{-3}, (c) 2.4×10^{-2}, (d) 3.6×10^{-2} M, (e) 6.0×10^{-2} M. Inset: Plot of C_0/A_{365} versus $1/C_g$ and the best-fit straight line.

Plotting C_0/A_{420} against $1/C_g$ gives a linear behavior (see inset of Figure 3), confirming the assumption of the formation of 1:1 enol/ACID and keto/ACID complexes. According to the intercept of 0.0025 M, K_b was calculated to be 0.15, and a value of 1.2×10^4 for K_a was deduced from the slope. Consequently, $\Delta G°$ values were calculated to be −5.56 and 1.12 kcal/mol for the enol + ACID → enol/ACID and enol/ACID → keto/ACID reaction, respectively, at room temperature. The equilibrium constants as well as other thermodynamic properties tuned by adding other types of guest molecules such as ACH, forming 3HIQ CDHB complexes, are shown in Table 1.

To emphasize the role of the CDHB formation contributing to the ground-state tautomerization in 3HIQ, we have studied the 3HIQ/guest complex involving a single hydrogen-bond formation. For this case, the TEA was chosen as a guest molecule. Since TEA possesses only a proton-accepting site, the 1:1 3HIQ/TEA complex, if it forms, should incorporate only a single hydrogen bond. Figure 4 shows absorption spectra of 3HIQ in cyclohexane as a function of the added TEA concentration. The appearance of a shoulder in the region of 350 nm indicates the formation of a enol−TEA hydrogen-bonded complex. However, since it requires a much higher concentration of amine to achieve the same absorbance (e.g. at 350 nm) as in the case of the enol/ACID complex, the association constant must be smaller than those of enol/guest CDHB complexes. In addition, under the sensitivity limit of our detecting system, the 420-nm absorption band associated with the S_0-S_1 transition of the keto/guest complex was not detectable. In other words, the single hydrogen bond facilitates only the formation of the enol/TEA complex in the ground state; while the enol/TEA → keto/TEA tautomerization is still a highly endergonic process and is not favorable at room temperature. On the basis of an equilibrium between the enol monomer and the 1:1 enol/TEA complex a Benesi−Hiderbrand plot at the 370-nm absorbance can be deduced and depicted in eq 5.

$$\frac{C_0}{A_{370}} = \frac{1}{\epsilon_{370} l K_a} \frac{1}{C_g} + \frac{1}{\epsilon_{370} l} \tag{5}$$

Applying eq **5** to our data gives a linear behavior, and K_a was calculated to be 0.15×10^2. The corresponding $\Delta G°$ value of −1.60 kcal/mol is less exergonic than half of the enol/enol and enol/ACID CDHB complex, providing indirect evidence that in addition to the hydrogen-bonding strength the CDHB formation may further stabilize the electronic energy of 3HIQ in the complex.

Fluorescence Spectra

3HIQ Self-Association. Table 1 lists the steady-state spectral properties of absorption and emission as well as relaxation dynamics for 3HIQ and its hydrogen-bonded species in cyclohexane. When the concentration of 3HIQ was prepared as low as 5.0×10^{-6} M in cyclohexane, a strong, normal Stokes-shifted emission ($\Phi_f \approx 0.27$) was observed with a peak maximized at

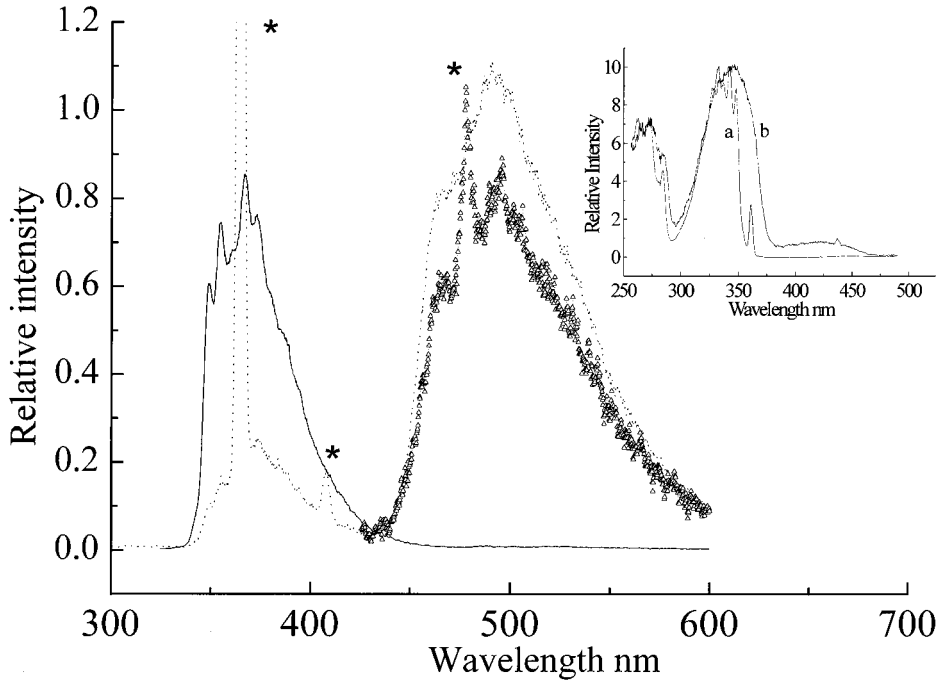

Figure 5. Fluorescence spectra of 3HIQ in cyclohexane with a concentration of (solid line) 5.0×10^{-6} M ($\lambda_{ex} = 340$ nm), (dashed line) 1.2×10^{-4} M ($\lambda_{ex} = 365$ nm), and (open triangle) 1.2×10^{-4} M ($\lambda_{ex} = 420$ nm). Inset: Excitation spectrum of 3HIQ (1.2×10^{-4} M in cyclohexane) monitored at (a) 360 nm and (b) 500 nm. * denotes the Raleigh and Raman scattering.

370 nm. The lifetime was measured to be 6.62 ns and was independent of the excitation as well as the monitored emission wavelength. Therefore, at a sufficiently low concentration of 3HIQ only one emitting species exists in the excited state, which is unambiguously assigned to the excited enol monomer. At a moderately high concentration, for example, 1.2×10^{-4} M, the steady-state fluorescence spectra of 3HIQ as a function of the excitation wavelength are shown in Figure 5. Upon excitation in the region of 420 nm, in which only the keto/enol complex absorbs, a normal Stokes-shifted fluorescence maximum at 490 nm was observed. The spectral features are an image of the 420-nm absorption band, leading us to conclude that the 490-nm emission is associated with the keto-like chromophore. Dual emission maxima at 370 (the F_1 band) and 490 nm (the F_2 band) were observed upon excitation at <365 nm. The intensity ratio for the F_1 band versus the F_2 band shows the excitation-wavelength dependence, indicating that the dual emission originates from various species of 3HIQ in ground-state equilibria. The assignment of various distinct emitting species can be partially resolved by the fluorescence excitation spectra (see inset of Figure 5). At the region of 360−400 nm (the F_1 band), the excitation spectrum is independent of the monitored emission wavelength and exhibits a structural excitation spectrum maximum at 340 nm. Due to its identity with respect to the absorption spectrum of the enol monomer, the conclusion that the F_1 band results exclusively from the excited enol monomer is unambiguous. In comparison, an ∼10-nm red-shifted structureless excitation spectrum ($\lambda_{max} \approx 350$ nm) as well as a broad 420-nm band was observed when the emission wavelength was monitored within the region of the F_2 band (e.g. 500 nm; see inset of Figure 5). The spectral features of the 350-nm band resemble the growing portion of the absorption spectrum upon increasing 3HIQ in cyclohexane (see Figure 2), and it is thus tentatively ascribed to the excitation spectrum of the enol dimer. The result clearly indicates that for the enol dimer a proton-transfer reaction takes place in the excited state, giving rise to a (keto*)/keto emission (* denotes the electronically excited state). This process, similar to that observed in 7AI dimer,[29−31] may involve the transfer of two protons, cooperatively triggered by a CDHB formation. Since negligible normal emission attributed to the enol dimer was observed in the steady-state measurement, the rate of double proton transfer must be much faster than the radiative decay rate of the enol dimer. This viewpoint will be verified in the following time-resolved measurement.

On the other hand, the keto/enol CDHB complex consists of two individual chromophores, the keto and enol form, linked by dual hydrogen bonds. Therefore, upon the excitation at <365 nm, except for the enol dimer, the enol part of the keto/enol CDHB complex should also be excited, even though its concentration is only ∼1/50 of the enol dimer (vide supra). The observation of the predominant keto emission leads us to conclude that an unusual relaxation pathway also takes place for the case of the keto/(enol*) complex. One possible mechanism incorporates a keto/(enol*) → enol/(keto*)‡ ($\ddagger$ denotes the highly vibrational state) double proton-transfer reaction, followed by a fast vibronic relaxation process, resulting in the enol/(keto*) emission. Alternatively, a mechanism incorporating an energy-transfer process from the keto/(enol*) to the (keto*)/enol complex through the short hydrogen-bonding distance cannot be eliminated. Although the enol emission resulting from the keto/(enol*) species was not observed experimentally, on the basis of Franck−Condon principle, it is reasonable to predict that the emission would be in the region of 380−400 nm, which should have a good spectral overlap with respect to the absorption band of the keto form, fulfilling the requirement of the energy-transfer mechanism. Since both mechanisms give rise to an identical product (i.e. the (keto*)/enol species) with an ultrafast reaction rate, distinguishing which mechanism is more appropriate to describe the experimental result is not possible at this stage.

Although the F_1 band, that is, the enol monomer emission, exhibits single-exponential decay kinetics, the relaxation dynamics of the F_2 band are somewhat complicated. Upon 365-nm excitation, the decay rate monitored at the emission region of 500 ± 5 nm cannot be fit by single-exponential decay

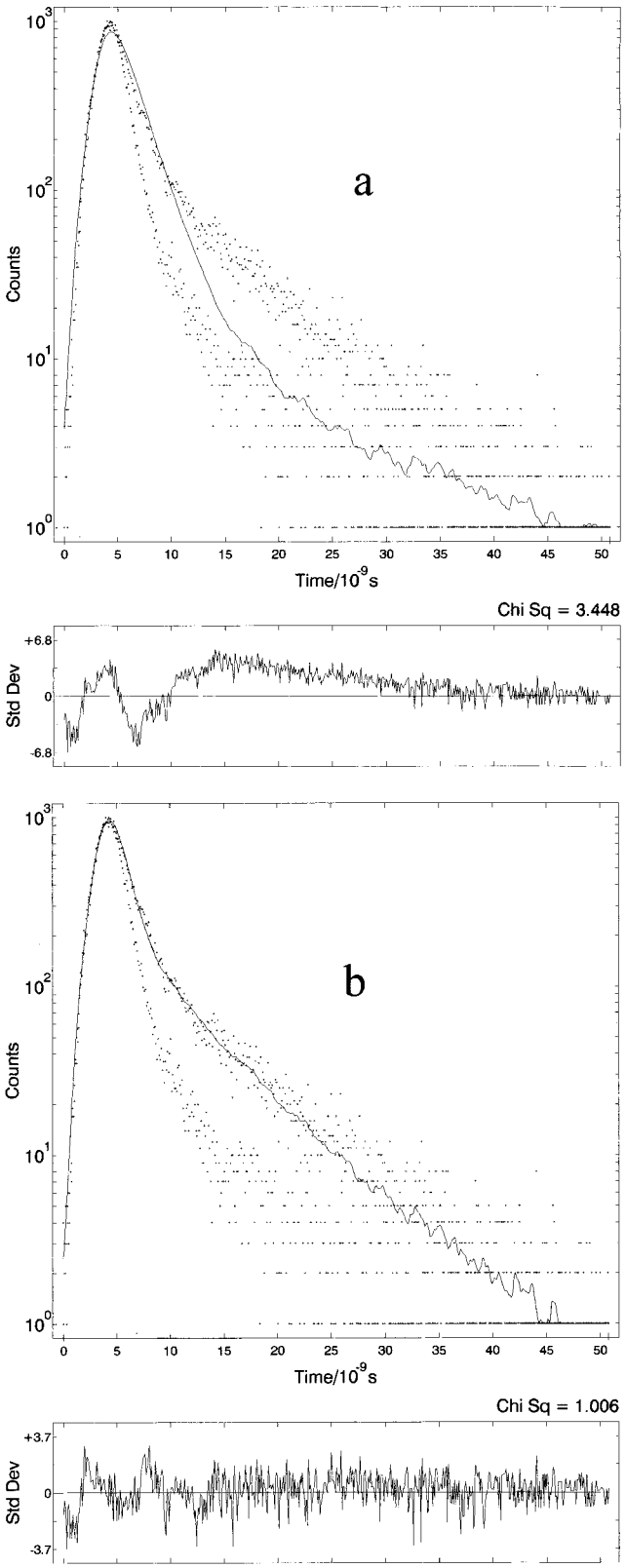

Figure 6. Time-dependent 500 nm (±5 nm) emission of 3HIQ (1.2×10^{-4} M in cyclohexane) fit by (a) one single-exponential decay (($\tau = 1.24 \times 10^9$ s, $\chi^2 = 3.448$) and (b) two single exponential decays ($k_1 = (1.72 \pm 0.06) \times 10^9$ s^{-1} ($\tau_1 = 0.58$ ns) and $k_2 = (1.58 \pm 0.05) \times 10^8$ s^{-1} ($\tau_2 = 6.34$ ns), $\chi^2 = 1.006$).

dynamics. Instead, it is well-fit by a double-exponential decay (see Figure 6), which is theoretically expressed as

$$F(t) = A_1 e^{-k_1 t} + A_2 e^{-k_2 t} \quad (6)$$

where A_1 and A_2 are the emission intensity at $t = 0$ for the decay components 1 and 2, respectively. While the intensity ratio for A_1 versus A_2 was excitation-wavelength-dependent, k_1 and k_2, within experimental error, were calculated to be constant with a fast and a slow component of $(1.72 \pm 0.06) \times 10^9$ s^{-1} ($\tau = 0.58$ ns) and $(1.58 \pm 0.05) \times 10^8$ s^{-1} ($\tau = 6.34$ ns), respectively, indicating the existence of two distinct decay species in the region of the F_2 band. Since the rise time for both components cannot be resolved, it is quite unlikely that one species is the precursor of the other. We therefore conclude that both (keto*)/keto and (keto*)/enol emitting species undergo different relaxation dynamics. Fortunately, which species is exactly attributed to the fast (or slow) component can be resolved from the direct excitation of the keto/enol species at 420 nm, resulting in the (keto*)/enol emission. The observed decay rate of $(1.65 \pm 0.08) \times 10^8$ s^{-1} ($\tau = 6.06$ ns), within experimental error, is identical with the slow component of the F_2 band upon excitation at 365 nm. Accordingly, the fast component is ascribed to the (keto*)/keto species. The result also gives definitive support for the assignment of the 420-nm keto-like absorption chromophore to the keto/enol complex rather than the keto dimer. If the keto dimer were the species in the ground-state equilibrium, its relaxation dynamics should be identical with that of the excited proton-transfer tautomer of the enol dimer, that is, the (keto*)/keto species. As a result, single-exponential decay dynamics should be observed, contradicting to the experimental result.

3HIQ/Guest CDHB Complexes. In comparison to the fluorescence spectra of 3HIQ self-associated species, the assignment of various emitting species is relatively straightforward for the case of the 3HIQ/ACID CDHB complex. Excitation within the absorption region of either the enol/ACID or the keto/ACID complex results in a unique keto-like emission band (the F_2 band) maximum at ~490 nm (see inset **B** of Figure 3). Unlike the complex relaxation dynamics in the case of self-association, the lifetime of the F_2 band can be well-fit by a single-exponential decay of $k_f = (1.42 \pm 0.08) \times 10^8$ s^{-1}, indicating that the enol/ACID complex, upon excitation, undergoes a fast proton-transfer reaction, resulting in the keto*/ACID species, which is identical with the directly excited (e.g. 420 nm) keto/ACID species existing in the ground-state equilibria.

The carboxylic acid assisted double proton transfer can be specified as a catalytic process since the molecular structure of the guest molecules, i.e., the acid functional group, remains unchanged. On the other hand, for the 3HIQ self-association, the double proton transfer for the single-photon-excited enol dimer results in the (keto*)/keto form consisting of an excited and an unexcited keto form. In this case, each enol part of the enol dimer does not mutually act as a catalyst but rather a reactant. A similar viewpoint has been addressed in the self-assisted proton-transfer reaction in 7-azaindole.[20,29,30] However, a significant difference between these two molecules is that 7-azaindole exists exclusively as the normal form in both gas and condensed phases. Thus, the proton-transfer tautomer of 7-azaindole has to be prepared in the excited state, of which the relaxation dynamics cannot be studied by the direct excitation. On the other hand, due to the existence of the ground-state keto/guest complex in 3HIQ, the relaxation dynamics among each CDHB species may be distinguished, especially when the occurrence of the proton-transfer reaction is a noncatalytic process. A prototype example has been demonstrated in cases of (keto*)/enol and (keto*)/keto CDHB species. Another noncatalytic example could be the 3HIQ/ACH complex.

SCHEME 2

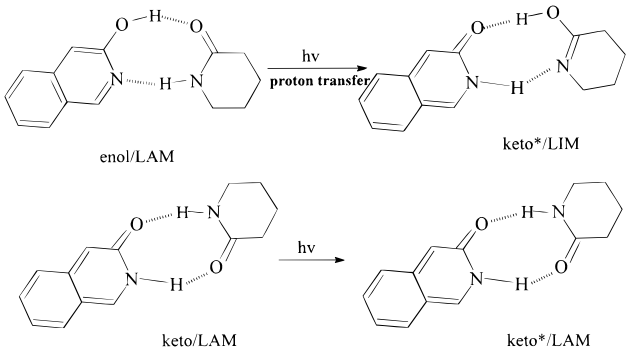

UV−vis absorption studies have revealed the existence of a ground-state equilibrium between enol/ACH and keto/ACH CDHB species (see Table 1). However, analyses of emission spectra indicate that the excitation of either species gives rise to keto-like emission exclusively. Since ACH exists predominantly as the lactam form (LAM) in the ground state, the occurrence of the excited-state proton-transfer reaction in the (enol*)/LAM complex should result in the (keto*)/LIM state (LIM denotes the lactim form of ACH; see Scheme 2), which may have quite different relaxation dynamics from the (keto*)/LAM state upon directly exciting the keto/LAM species. However, regardless of the excitation wavelength, the F_2 band can only be fit by a single-exponential decay rate of $(1.2 \pm 0.2) \times 10^8$ s^{-1}, indicating that the decay dynamics for both (keto*)/LAM and (keto*)/LIM are similar; at least they cannot be resolved under the resolution of our detecting system. This result contrasts with those of the 3HIQ self-association species in which both (keto*)/keto and (keto*)/enol species undergo drastically different decay dynamics. In later sections we will tentatively rationalize the results by a correlation between the dynamics of quenching in the excited state and the relative hydrogen-bonding strength for each 3HIQ CDHB species. Finally, for all 3HIQ/guest CDHB complexes studied, the rise time of the F_2 band cannot be resolved, indicating that the rate of double proton transfer in the excited state is much greater than our system response limit of 5.0×10^9 s^{-1} at ambient temperature.

Theoretical Approach. We have carried out a theoretical approach to verify our experimental results. Table 2 lists the calculated formation of enthalpy, entropy, and consequently the free energy among the geometry-optimized monomer, the CDHB dimer, and complexes of 3HIQ. Figure 7a−e depicts the full geometry optimized structures (6-31G* basis set) of 3HIQ and its self-associated species. The calculated free energy of formation shows that the enol monomer of 3HIQ is more stable than the keto monomer by 9.5 kcal/mol. The result indicates that the enol monomer form should be a predominant species in the gas phase, consistent with the experimental observation. Several remarks can be pointed out from the results of Figure 7 in combination with Table 2. First, for the case of self-association a surprisingly large association enthalpy, ΔH_{ac}, of −17.58 kcal/mol was calculated for the keto dimer which is >7 kcal/mol more exothermic than that of −8.42 and −10.04 kcal/mol for the enol dimer and the enol/keto complexes, respectively. Since ΔH_{ac} generally correlates well with the hydrogen-bonding strength, the result may simply indicate that the hydrogen-bonding strength is on the order of keto dimer > keto/enol complex > enol dimer. Evidence can be given by the calculated hydrogen-bonding distance of 1.815 Å in the case of the keto dimer, which is 0.148 Å shorter than that of the enol dimer (see Figure 7). ΔH_{ac} values were also estimated to be −7.66 and −9.71 kcal/mol for the formation of enol complexes with ACH and ACID, respectively, which linearly correlates with the experimentally measured order of the association constants for various enol/guest complexes (see Table 1), indicating that the hydrogen-bonding strength is a key factor to fine-tune the stability of 3HIQ CDHB species. The calculation also shows a strong correlation between ΔH_{ac} and the relative change in bond distances for the enol (or keto) complex in comparison with its corresponding monomer. In comparison with the enol monomer, the C(1)−N(2), C(3)−C(4), and C(9)−C(10) bond distances increase, while the C(3)−O, C(1)−C(10), and C(4)−C(9) bond distances decrease on formation of the enol/guest complexes (see Table 3). In addition, both an increase and decrease of the double-bond character are in the order enol/keto > enol/ACID > enol dimer > enol/ACH, which linearly corresponds to the decreasing exothermicity of the calculated ΔH_{ac} among the four enol CDHB complexes. A similar correlation was also observed for the keto/guest CDHB complexes, suggesting a cooperative change in the electronic configuration of 3HIQ mediated by the conjugated hydrogen-bonding formation, resulting in an unusually large association.

Second, the results qualitatively predict the correct trend for the relative stability between each CDHB species. For example, the enol dimer was calculated to be the most stable species among the three self-association forms, in agreement with the experimental observation. In addition, the calculation also predicts the enol/keto complex to be more stable than the keto dimer by ∼3.0 kcal/mol, supporting the assignment of the keto-like absorption to the enol/keto complex in the earlier sections. Furthermore, for all 3HIQ/guest complexes studied, Table 2 predicts the enol/guest complex to be more stable than its corresponding keto/guest complex, consistent with the experimental results. However, it should be noted that the calculated absolute free energies for all the 3HIQ CDHB species studied deviate from the experimental values generally by 4−7 kcal/mol. For instance, the free energy of formation for the enol dimer is calculated to be 1.9 kcal/mol more than that of two separated enol species, while a value of −5.36 kcal was obtained experimentally. On the other hand, the free-energy change of the enol dimer → keto/enol proton-transfer tautomerism was theoretically estimated to be 7.62 kcal/mol, which is far from the experimental value of 2.29 kcal/mol at room temperature. Although the use of a lower basis set may introduce certain deviations, the major discrepancy between the theoretical (in gas phase) and experimental (in solution) approaches is believed to be due to solvation energy in the solution phase. Especially for the case of the enol/keto complex ($\mu = 1.3$ D) in which the solute (dipole)−solvent (induced dipole) interaction should result in a significantly larger solvent-stabilization energy than that for both enol and keto dimers, of which the net dipole moments are calculated to be 0. Unfortunately, due to the complicated molecular structure of the CDHB species, at this stage, it is not possible to calculate the solvation energy based on an ab initio approach. We have also attempted to resolve the solvation energy based on several different semiempirical methods. However, results are scattered, possibly due to the programs we applied that are based on the continuum dielectric model cannot accurately describe the 3HIQ hydrogen-bonded systems in solution. Furthermore, the entropy calculation is based on an infinitely diluted solute in which the correction term for the entropy due to the concentration effect has been neglected. Such an effect is significant for experiments using a finite concentration, leading to a more favorable entropy upon the CDHB formation.

TABLE 2: Thermodynamic Properties of 3HIQ and Its CDHB Species in the Gas Phase Calculated by the RHF/6-31G* Basis Set at 298K[a,b]

	total *E*	*H*	*S*	*G*	BSSE	ΔH_{ac}	$\Delta G°$
enol	−474.233 57	−474.087 10	84.674	−474.127 33			0
keto	−474.218 5	−474.071 74	85.041	−474.112 15			9.52
enol/enol	−948.485 69	−948.190 37	134.615	−948.254 33	−1.73	−8.42	1.94
keto/keto	−948.471 26	−948.175 51	133.282	−948.238 84	−2.52	−17.58	12.45
enol/keto	−948.473 44	−948.178 04	135.932	−948.242 63	−2.01	−10.04	9.56
enol/ACID	−702.075 86	−701.861 32	113.625	−701.915 70	−1.96	−9.71	1.56
keto/ACID	−702.069 90	−701.854 29	116.768	−701.909 77	−2.38	−14.52	5.70
enol/LAM	−798.183 66	−797.889 75	129.388	−797.951 23	−1.92	−7.66	2.28
keto/LAM	−798.178 01	−797.883 63	127.430	−797.944 17	−2.38	−12.99	7.17
keto/LIM	−798.157 13	−797.86331	126.031	−797.923 19	−2.3	−12.42	20.25
enol/TMA[c]	−647.529 01	−647.255 87	123.425	−647.314 51	−1.98	−4.30	5.07
keto/TMA	−647.515 65	−647.242 13	121.554	−647.299 89	−2.32	−4.97	14.58

[a] Total energy, enthalpy, and free energy in hartrees, entropy in cal mol^{-1} K^{-1}, ΔE_{cp}(BSSE) in kcal/mol. [b] $\Delta G°$ values for various self-association forms were calculated relative to two enol monomers. while $\Delta G°$ for all other CDHB complexes was calculated by the difference between the free energy of the CDHB complex and those of enol plus guest molecules. [c] To avoid the complexity, trimethylamine (TMA) was used instead of TEA in the calculation.

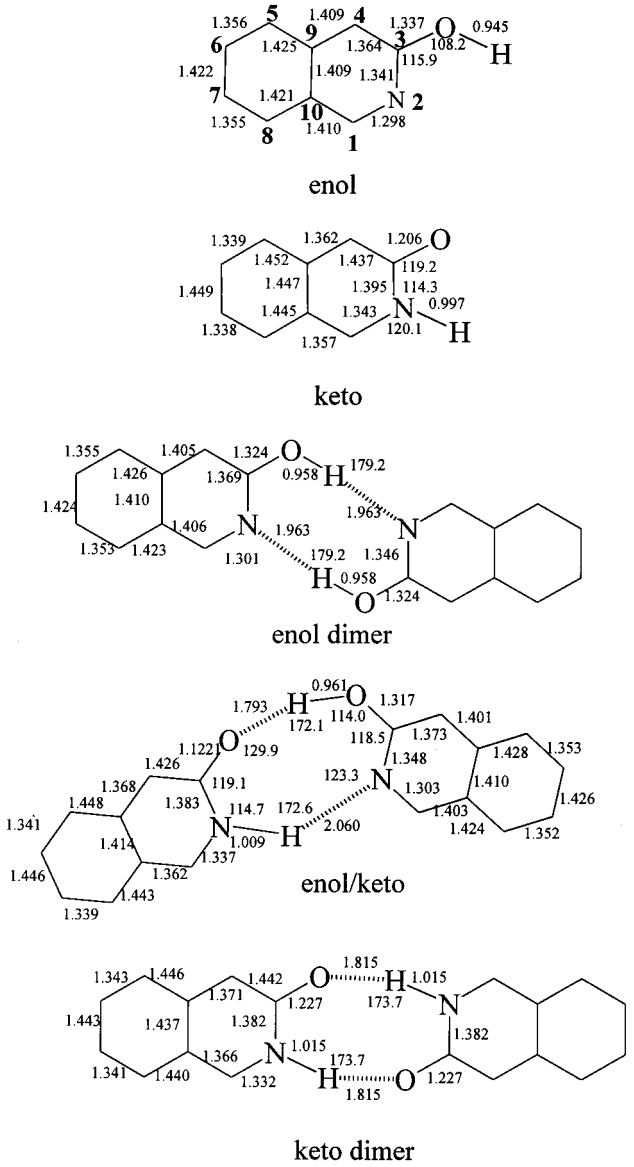

Figure 7. Optimized geometries based on the HF/6-31G* basis set (in Å and deg, only critical angles are shown) for the ground states of 3HIQ (a) enol, (b) keto, (c) enol dimer, (d) enol/keto, and (e) keto dimer.

Nevertheless, the theoretically calculated relative free energy serves as a good reference to predict the shift of the enol−keto equilibria as a function of the added guest molecule. The change of free energy for enol/enol → keto/enol, enol/LAM → keto/LAM, and enol/ACID → keto/ACID tautomerism was calculated to decrease on the order 7.62, 4.89, and 4.14 kcal/mol, respectively. This trend qualitatively rationalizes the increase of the equilibrium constant toward the keto form from the self-association to 3HIQ/ACID experimentally (see Table 1). For the case of the 3HIQ/TMA single hydrogen-bonded complex the calculation shows a highly endergonic enol/TMA → keto/TMA reaction of 9.51 kcal/mol. The result predicts the nonexistence of the keto/TMA complex, consistent with the experimental observation.

TABLE 3: Relative Distances (in Å) for Some Crucial Bonds in 3HIQ Enol and Its Corresponding Dimer and Complexes[a]

	C1−N2	C3−C4	C9−C10	C3−O	C1−C10	C4−C9
enol (1)	1.298	1.364	1.409	1.337	1.411	1.409
enol dimer (2)	1.301	1.369	1.410	1.324	1.406	1.405
Δd (2) − (1)	0.003	0.005	0.001	−0.013	−0.005	−0.004
enol/LAM (6)	1.301	1.370	1.410	1.319	1.405	1.403
Δd (6) − (1)	0.003	0.006	0.001	−0.018	−0.006	−0.006
enol/ACID (4)	1.303	1.370	1.410	1.319	1.403	1.403
Δd (4) − (1)	0.005	0.006	0.001	−0.018	−0.008	−0.006
enol/keto (3)	1.303	1.373	1.410	1.317	1.403	1.401
Δd (3) − (1)	0.005	0.009	0.001	−0.02	−0.008	−0.008
enol/BHP (5)	1.305	1.373	1.411	1.316	1.401	1.401
Δd (5) − (1)	0.007	0.009	0.002	−0.021	−0.01	−0.008

[a] The same numbering sequence for the atoms as Figure 7.

Discussion

In studying the 3HIQ self-association, it is important to note that the ratio of the relative intensity for I_{420} versus I_{365} (subscript denotes the excitation wavelength in nm) in the excitation spectrum is drastically different from the absorbance ratio for A_{420} versus A_{365}. The value of (I_{420}/I_{365}) was measured to be ∼0.13 (see inset of Figure 5), whereas (A_{420}/A_{365}) was measured to be as small as 0.017 (see Figure 2). Since the excitation spectra have been corrected (see the Experimental Section), the difference resulting from the wavelength-dependent response of the detecting system can be excluded. Therefore, the result indicates that the fluorescence yield is excitation-wavelength-dependent, giving a smaller yield by exciting the enol dimer than the keto/enol complex. One possible interpretation is that the excited-state proton-transfer reaction for the enol dimer is not solely adiabatic, and a nonradiative proton-transfer process from the excited enol dimer to the ground-state keto dimer may occur. Such a process, induced by the hydrogen-bonding effect, should be fast enough in order to compete with the adiabatic proton-transfer reaction. However, for most molecules exhibit-

ing a highly unsymmetric excited-state proton-transfer reaction, the process has been concluded to be associated with a small or negligible energy barrier and the proton-transfer rate may be mainly governed by the tunneling mechanism, which has been generally reported to be on the order of $>10^{11}$ s^{-1} for many compounds.[31−36] Therefore, although the proposed ultrafast nonadiabatic proton-transfer rate cannot be eliminated at this stage, it seems to contradict the widely accepted theory. Alternatively, a more plausible mechanism based on the different fluorescence yields between the excited keto dimer and the keto/enol complex was proposed. In the cyclohexane solution containing 1.0×10^{-4} M 3HIQ, upon 365-nm excitation, a double-exponential fit of the fluorescence decay at 500 ± 5 nm gives the preexponential factors A_1 and A_2 of 0.16 and 0.006 for the keto dimer and keto/enol complexes, respectively. Thus, the percentage of the keto dimer emission intensity, τ_1 (%), that contributes to the overall 500-nm emission intensity is expressed as

$$\tau_1\,(\%) = \frac{A_1\tau_1}{A_1\tau_1 + A_2\tau_2} \tag{7}$$

which has been experimentally calculated to be 73.2%. Since the observed decay dynamics are based on the time-dependent fluorescence intensity, τ_1 (%) is thus theoretically derived to be

$$\tau\,(\%) = \frac{\alpha k_{1r}[(\text{keto})_2^*]_0\tau_1}{\alpha k_{1r}[(\text{keto})_2^*]_0\tau_1 + \alpha k_{2r}[(\text{keto})^*/\text{enol}]_0\tau_2} = 0.737 \tag{8}$$

where α is the instrument factor, including sensitivity, alignment, etc., of the detecting system. k_{1r} and k_{2r} are radiative decay rates for the keto dimer and keto/enol complex, respectively. Subscript 0 denotes the concentration of each excited species at $t = 0$. In eq 8, it is reasonable to assume that the radiative decay rate of the 3HIQ keto form is similar for various keto CDHB complexes. This viewpoint can be supported by the nearly solvent-independent absorption cross section and spectral feature for the keto form. For example, the ϵ value at peak maximum (420 nm) of the keto/enol complex has been estimated to be 2910 M^{-1} cm^{-1} in cyclohexane (vide supra), which is similar to the that of ~2950 M^{-1} cm^{-1} for the solvated keto form in H_2O. As a result, eq 8 can be simplified to

$$\tau\,(\%) = \sim\frac{[(\text{keto})_2^*]_0\tau_1}{[(\text{keto})_2^*]_0\tau_1 + [(\text{keto})^*/\text{enol}]_0\tau_2} = 0.737 \tag{9}$$

Plugging τ_1 and τ_2 values (see Table 1) into eq 9, $[(\text{keto})_2^*]_0/[(\text{keto})^*/\text{enol}]_0$ was then calculated to be 26.63. Since the absorbance for either the enol dimer or keto/enol complex was kept smaller than 0.1 throughout the study, both $[(\text{keto})_2^*]_0$ and $[(\text{keto}^*)/\text{enol}]_0$ are proportional to the absorbance of the enol dimer and (keto/enol) complex, respectively, that is, the concentration of enol dimer ($[(\text{enol})_2]$)and keto/enol complex ($[(\text{keto/enol})]$), assuming that the absorption cross section is the same at 365 nm for these two species. Accordingly, a value of $[(\text{enol})_2]/[(\text{keto/enol})] = 26.63$ was obtained, which corresponds to a K_b value of 0.035, in good agreement with the value of 0.021 measured from the absorption measurement. When monitoring at 500 nm, the ratio for the excitation intensity $I_{420\ nm}$ versus $I_{365\ nm}$ is theoretically calculated to be

$$\frac{I_{420}}{I_{365}} = \frac{[(\text{keto}^*)/\text{enol}]_0\tau_2(\lambda_{ex} = 420\text{nm})}{[(\text{keto}^*)/\text{enol}]_0\tau_2(\lambda_{ex} = 365\text{nm}) + [(\text{keto})_2^*]_0\tau_1(\lambda_{ex} = 365\text{nm})} = \frac{\epsilon_{420}\,[(\text{keto/enol})]\tau_2}{\epsilon_{365}\,[(\text{keto/enol})]\tau_2 + \epsilon_{365}\,[(\text{keto})_2]\tau_1}$$

Taking ϵ_{420} and ϵ_{365} to be 2910 and 3200 M^{-1} cm^{-1}, respectively, I_{420}/I_{365} was calculated to be 0.25, in good agreement with the steady-state measurement of 0.13 (see inset of Figure 5). The results strongly support the proposed mechanism that the excitation of the enol dimer and keto/enol complex results in keto*/keto and keto*/enol forms, respectively, which undergo drastically different relaxation dynamics, hence the different fluorescence yields. We have also attempted to resolve keto*/keto and keto*/enol emission bands by the time-resolved spectral evolution technique. Figure 8a shows the emission spectrum obtained by integrating the photon-counting signal in the time delay interval of 0−1.5 ns. It is apparent that the resulting spectrum which has a maximum at ~490 nm, within the experimental error, is overlapped with that obtained at a time delay of >5.0 ns (Figure 8b). The result suggests that regardless of the remarkably different CDHB strength, the S_0-S_1 energy gap is similar for both keto/keto and keto/enol species, indicating that the hydrogen-bonding effect may play an equivalent role in both ground and excited states.

In summary, Scheme 3 depicts the overall proton-transfer tautomerism for the case of 3HIQ self-dimerization in both ground and excited states. In cyclohexane, spectral analyses conclude the existence of equilibria between various proton-transfer tautomers, including the enol monomer, enol dimer (or 1:1 enol/guest complex), and keto/enol complex (or 1:1 keto/guest complex). An ultrafast excited-state proton-transfer reaction takes place in the enol dimol, resulting in a (keto*)/keto species. Further proton transfer from the (keto*)/keto to the (keto*)/enol species, being thermodynamically allowed, is a dynamically prohibited process due to a highly strained activation energy, which should be on a time scale much slower than the decay rate of the (keto*)/keto species. Both (keto*)/keto and (keto*)/enol emissions are spectrally indistinguishable but undergo drastically differently relaxation dynamics, being faster in the (keto*)/keto species possessing a stronger CDHB strength. It should be also noted that in Scheme 3 the tautomerism from the enol dimer to the keto/enol complex is prohibited by a direct proton-transfer reaction. This process, however, may be thermodynamically accomplished by a series of steps incorporating association, proton-transfer, and association reactions in the ground state depicted as follows.

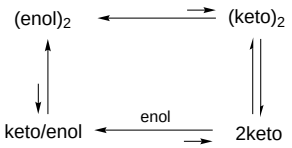

The weak emission of the keto/guest complex can be interpreted in terms of two possible deactivation mechanisms associated with the hydrogen bond. Since the S_1-S_0 emission (~20 000 cm^{-1}) of the keto tautomer species is relatively small, the nonradiative pathway quenching through electronic energy transfer coupled with the O−H (or N−H) stretching vibrations of the molecules is plausible. High-frequency O−H or N−H vibrations are good acceptors because fewer quanta are required

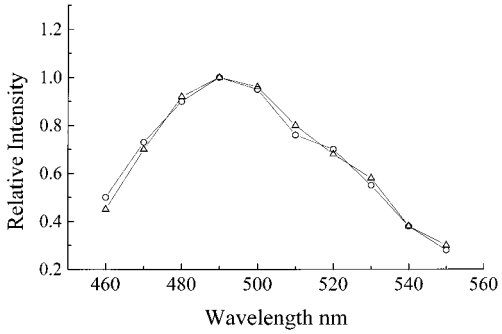

Figure 8. Time-dependent spectral evolution (460−550 nm, $\lambda_{ex} = 365$ nm) of 3HIQ (1.2×10^{-4} M) in cyclohexane. The spectra were taken by integrating the signal intensity within a time window of (○) 0−1.5 and (△) 5.0−10.0 ns and normalized at 490 nm. In this study the spectral resolution was measured to be ∼8.0 nm. In comparison with the steady-state emission spectrum (see Figure 5), the spectral distortion in the region of <480 nm is due to the insertion of a long-wavelength band-pass filter (Schott GG 455) in front of the emission slit.

SCHEME 3

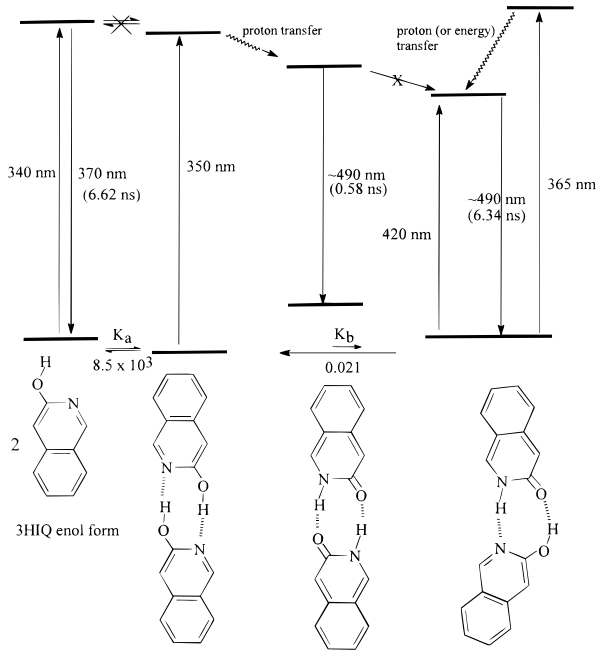

in S_0 than for a lower frequency vibration, thus providing a more favorable Franck−Condon factor for the S_1-S_0 radiationless process. Apparently, deuterium substitution lowers the frequency of the acceptor mode and hence decreases the Franck−Condon factor and the nonradiative rate. To elucidate this possible mechanism, we have performed a series of experiments to study the deuterium isotope effect and found that there is negligible isotope effect upon the complex formation between the deuterium-substituted 3HIQ and the deuterated guest molecules, eliminating this proposed mechanism. Alternatively, it is more likely that the small-frequency vibrational modes associated with the intermolecular hydrogen-bonding interaction play a key role in inducing the radiationless transition. For this case, the hydrogen-bonding strength should be directly coupled with the nonradiative deactivation pathway. This proposed mechanism can be rationalized by the theoretical approach in which the association energy (ΔH_{ac}) of the keto dimer was calculated to be ∼8 kcal/mol more exothermic than the keto/enol complex in the ground state. Assuming a similar difference of ΔH_{ac} for these two species in the excited state, the result suggests that the hydrogen-bonding strength in the (keto*)/keto CDHB complex is much stronger than that in the (keto*)/enol complex. As a result, a faster radiationless deactivation is expected for the (keto*)/keto species, consistent with the experimental result. Further support of the CDHB strength-dependent relaxation dynamics can be given in the case of 3HIQ/ACH complex. Due to the nearly identical ΔH_{ac} values (see Table 2), the CDHB strength is assumed to be the same for both keto/LAM and keto/LIM species. Assuming similar hydrogen-bonding properties in the excited state, the indistinguishable relaxation dynamics between (keto*)/LAM and (keto*)/LIM species can thus be rationalized by their nearly identical CDHB strength (see Table 2).

Conclusion

Summarizing the above experimental and theoretical results, we conclude that in the ground state, from the thermodynamic point of view, the CDHB formation and its strength play a key role to fine-tune the enol−keto tautomerization in cyclohexane, which is otherwise exclusively favorable to the enol form without the CDHB formation. In the excited state, the CDHB formation dynamically plays a major role to facilitate the enol−keto tautomerization in 3HIQ, which is otherwise prohibited during the life span of the excited enol monomer due to the steric effect, that is, the high strain energy for the proton-transfer reaction in a four-member-ring system. However, whether the CDHB formation contributes to the thermodynamic factor of the reaction, that is, the stabilization energy between reactant (the enol form) and product (the keto form) in the excited state is not important since for the 3HIQ CDHB species, the enol−keto tautomerization is a highly endergonic process and the rate of excited-state double proton transfer is fast, with a lower limit of 5×10^9 s^{-1}. Although the significance is only based on a simple molecular model, it clearly implicates that the tautomerization assisted by the CDHB or even conjugated multiple hydrogen bonding (CMHB) formation may also be feasible in a biological system. We expect that the CMHB formation, to a certain extent, may induce charge redistribution of the chromophore significantly, particularly when molecules have cooperative electron-donating and -accepting functional groups. Therefore, studies of various DNA base pairs intercalated by guest molecules with the cooperative multiple-hydrogen-bonding formation may be crucial, which may provide valuable information relating to the mutation of DNA at the molecular level.

Acknowledgment. Startup support from the National Chung-Cheng University is graciously acknowledged. This work was supported by the National Science Council, Taiwan, ROC (Grant No. NSC 87-2119-M-194-002). We thank the National Center for High-Performance Computing, Taiwan, for the use of their facility. We also thank Professor Shannon Martinez for many helpful discussions.

References and Notes

(1) Ingham, K. C.; El-Bayoumi, M. A. *J. Am. Chem. Soc.* **1971**, *93*, 5023.
(2) Ingham, K. C.; El-Bayoumi, M. A. *J. Am. Chem. Soc.* **1974**, *96*, 1674.
(3) Douhal, A.; Kim, S. K.; Zewail, A. H. *Nature* **1995**, *378*, 260.
(4) Beak, P.; Fry, F. S. Jr.; Lee, J.; Steele, F. *J. Am. Chem. Soc.* **1976**, *98*, 171.
(5) Beak, P. *Acc. Chem. Res.* **1977**, *10*, 186.
(6) (a) Beak, P.; Covongton, J. B.; White, J. M. *J. Org. Chem.* **1980**, *45*, 1347. (b) Beak, P.; Covongton, J. B.; White, J. M.; Zeigler, J. M. *J. Org. Chem.* **1980**, *45*, 1354.
(7) Hammes, S. G.; Park, A. C. *J. Am. Chem. Soc.* **1969**, *91*, 956.
(8) Kuzuya, M.; Noguchi, A.; Okuda, T. *Bull. Chem. Soc. Jpn.* **1984**, *57*, 3454.

(9) Millefiori, S.; Millefiori, A. *Bull. Chem. Soc. Jpn.* **1990**, *63*, 2981.
(10) Fabian, W. M. F. *J. Phys. Org. Chem.* **1990**, *3*, 332.
(11) Cieplak, P.; Bash, P.; Chandra, S. U.; Kollman, P. A. *J. Am. Chem. Soc.* **1987**, *109*, 6283.
(12) Field, M. J.; Hiller, I. H. *J. Chem. Soc., Perkin Trans. 2*, **1987**, 619.
(13) Kwiatkowski, J. S.; Bartlett, R. J.; Person, W. B. *J. Am. Chem. Soc.* **1988**, *110*, 2353.
(14) Adamowicz, L. *Chem. Phys. Lett.* **1989**, *161*, 73.
(15) Karelson, M. M.; Katritzky, A. R.; Szafran, M.; Zerner, M. C. *J. Org. Chem.* **1989**, *54*, 6030.
(16) Moreno, M.; Miller, W. H. *Chem. Phys. Lett.* **1990**, *171*, 475.
(17) Wong, M. W.; Wiberg, K. B.; Frisch, M. J. *J. Am. Chem. Soc.* **1992**, *114*, 1645, and references therein.
(18) Chou, P. T.; Wei, C. Y.; Hung, F. T. *J. Phys. Chem.*, in press.
(19) Evans, D. A.; Smith, G. F.; Wahid, M. A. *J. Chem. Soc. (B)* **1976**, 590.
(20) Chang, C. P.; Hwang, C. W.; Kuo, M. S.; Chou, P. T.; Clement, J. H. *J. Phys. Chem.* **1994**, *98*, 8801.
(21) Demas, J. N.; Crosby, G. A. *J. Phys. Chem.* **1971**, *75*, 991−1024.
(22) (a) Wang, J.; Boyd. R. J. *Chem. Phys. Lett.*, **1996**, *259*, 647. (b) Wang, J.; Boyd, R. J. *J. Phys. Chem.* **1996**, *100*, 16141.
(23) Wong, M. W.; Wiberg, K. B.; Frisch, M. J. *J. Am. Chem. Soc.* **1992**, *114*, 1645.
(24) Stewart, J. J. P. *J. Comput. Chem.* **1989**, *10*, 221.
(25) Buemi, G. *THEOCHEM* **1988**, *41*, 379.
(26) Bliznyuk, A. A.; Voityuk, A. A. *THEOCHEM* **1983**, *41*, 343.
(27) Wimmette, H. J.; Linnell, R. H. *J. Phys. Chem.* **1962**, 66, 546.
(28) Fritzche, V. H. *Ber. Bunsen-Ges. Phys. Chem.* **1964**, *68*, 459.
(29) Chou, P. T.; Wei, C. Y.; Chang, C. P.; Kuo, M. S. *J. Phys. Chem.* **1995**, *99*, 11994.
(30) Chou, P. T.; Wei, C. Y.; Chang, C. P.; Chiu, C. H. *J. Am. Chem. Soc.* **1995**, *117*, 7259.
(31) Smirnov, A. V.; English, D. S.; Rich, R. L.; Lane, J. Teyton, L.; Schwabacher, A. W.; Luo, S.; Thornburg, R. W.; Petrich, J. W. *J. Phys. Chem. B* **1997**, *101*, 2758, and references therein.
(32) Laermer, F.; Elsaesser, T.; Kaiser, W. *Chem. Phys. Lett.* **1988**, *148*, 119.
(33) Wiechmann, M.; Port, H.; Laermer, F.; Frey, W.; Elsaesser, T. *Chem. Phys. Lett.* **1990**, *165*, 28.
(34) Frey, W.; Laermer, F.; Elsaesser, T. *J. Phys. Chem.* **1991**, *95*, 10391.
(35) Chudoba, C.; Riedle, E.; Pfeiffer, M.; Elsaesser, T. *Chem. Phys. Lett.* **1996**, *263*, 622.
(36) Pfeiffer, M.; Lau, A.; Lenz, K.; Elsaesser, T. *Chem. Phys. Lett.* **1997**, *268*, 258.